Cellulose (2019) 26:6241–6258
https://doi.org/10.1007/s10570-019-02531-9

ORIGINAL RESEARCH

Enhanced removal of prometryn using copper modified microcrystalline cellulose (Cu-MCC): optimization, isotherm, kinetics and regeneration studies

Zaharaddeen N. Garba · Weiming Zhou · Ibrahim Lawan · Mingxi Zhang · Zhanhui Yuan

Received: 30 January 2019 / Accepted: 24 May 2019 / Published online: 1 June 2019

Abstract In this work, we incorporated Cu^{2+} on to microcrystalline cellulose (MCC) powder by a simple synthesis method to produce a composite material (Cu-MCC) with its suitability in prometryn (Pr) adsorption tested from synthetic wastewater. Various characterization techniques were applied in studying the prepared Cu-MCC with response surface methodology applied in order to study the influence of adsorbent dosage, solution pH and shaking speed, which suggested a quadratic model for the response (Pr percentage removal). The optimum adsorption conditions obtained were adsorbent dosage of 0.40 g, solution pH of 11 and shaking speed of 215 rpm with the model adequacy and significance validated by ANOVA. Langmuir and pseudo-second order were the most appropriate models in describing the generated equilibrium and kinetic data, giving rise to a monolayer adsorption capacity value of 97.80 mg/g at room temperature. The desorption of Pr on Cu-MCC was also probed depicting the adsorption capacity to be about 66.7% of its initial value after six sequential adsorption–desorption cycles. Overall, the prepared Cu-MCC was revealed to have great potential for being a good adsorbent in the removal of water contaminants such as Pr, based on the obtained results.

Electronic supplementary material The online version of this article (https://doi.org/10.1007/s10570-019-02531-9) contains supplementary material, which is available to authorized users.

Z. N. Garba · W. Zhou · I. Lawan · M. Zhang · Z. Yuan (✉)
College of Materials Engineering, Fujian Agriculture and Forestry University, Fuzhou, China
e-mail: zhanhuiyuan@fafu.edu.cn

Z. N. Garba
Department of Chemistry, Ahmadu Bello University, Zaria, Nigeria

Graphic abstract

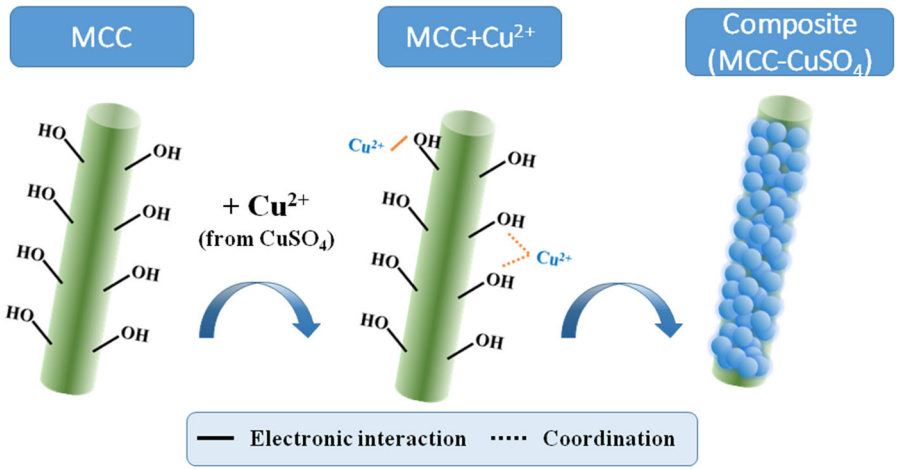

Keywords Microcrystalline cellulose · Prometryn · Optimization · Central composite design · Herbicide · Adsorption

Introduction

Negative consequences such as surface and groundwater pollution as well as soil and sediments contamination are always synonymous with the growing use of herbicides in agriculture (Grabka et al. 2015; Scribner et al. 2005). 2,4-bis(isopropyl amino)-6-(methylthio)-*s*-triazine popularly known as prometryn (Pr) is one of such herbicides that pose serious threat to the environment. It is a colorless crystal, classified as weakly polar, nonionic and hydrophobic compound (log $K_{ow} > 2$) belonging to the *s*-triazines group (Plakas and Karabelas 2009). Pr was majorly used in the control of broadleaf and grassy weeds, vegetables and other crops such as cotton, carrot and coriander (Grabka et al. 2015; Liu et al. 2018). As a result of the potential risk to environment as well as human and animal's health associated with it, European Union banned the use of Pr since 2014. But Pr is still available outside Europe in countries such as South Africa, United States, Canada, Australia and China (Velisek et al. 2015; Zhou et al. 2012).

In order to curtail water contamination by herbicides, various disposal methods ranging from physical (Brillas et al. 2003; Chuluun et al. 2009; Hladik et al. 2005; Krutz et al. 2003; Peña et al. 2011), biological (Brogan and Relyea 2013; Matby et al. 2009) as well as biotechnological (Kanissery and Sims 2011; Nawaz et al. 2011.) were reported to have been applied.

For decades, adsorption process has been reported as the most effective wastewater treatment method for various contaminants (Alidadi et al. 2018; Alizadeh et al. 2017; Bazrchi et al. 2018; Bouamra et al. 2018; Garba and Afidah 2014, 2015, 2016; Garba et al. 2015, 2016a). Activated carbon activated in distinct ways (Adetokun et al. 2019; Ayranci and Hoda 2005; Njoku et al. 2014; Salman and Hameed 2010a, b; Salman et al. 2011), nanotubes (Pyrzynska 2011; Pyrzynska et al. 2007), zeolites (Yonli et al. 2012), montmorillonites (Akçay et al. 2006; Park et al. 2011) and sepiolites (Akçay et al. 2005) were some of the numerous adsorbents reported to have been used.

Cellulose is a crystalline biopolymer possessing long chains of β-D-glucopyranose units joined by β-1,4-glycosidic linkage in which inter- and intramolecular hydrogen bonding restrict its main chain motion (Fahma et al. 2010; Gunny et al. 2017; Trache et al. 2016). MCC (an odourless, white crystalline powder) is an important derivative of cellulose (Das et al. 2010). Strong acid hydrolysis process is the most popular method employed in obtaining MCC from native cellulose (Jinbao et al. 2013; Vieira Ferreira et al. 2012). Some of the advantages associated with MCC include larger surface area, biocompatibility, low density, non-toxicity and biodegradability. Much cognizance was given to MCC especially in the last few years due to such properties it possesses (Trache et al. 2016). Such properties gave MCC the flexibility

to have been applied in various applications including adsorption as adsorbent for dye removal from water (Hussin et al. 2016).

To enhance the adsorption capacity and make MCC a better adsorbent, various chemical modifications of its surface were reported with pyridine diester and pyridine diacid (Sun et al. 2016), *N*,*N*-dimethyldodecylamine (Hu et al. 2014), aminoethanethiol (Silva et al. 2013), dithiooxamide (Jorgetto et al. 2013), pyrogallol (Gurnani and Singh 2004), 3-chloro-2-hydroxypropyl triethylammonium chloride (Hashem and El-Shishtawy 2001) and MnO_2 (Jiao et al. 2017) which improved its physical and chemical properties.

The usage of copper modified microcrystalline cellulose (Cu-MCC) in the adsorption of herbicides from synthetic wastewater constitutes the novelty of our work especially Pr herbicide. We chose MCC as favorable material for our adsorbent due to it possessing nanoporous surface, renewability, environmental friendliness, cheap and readily available (Miao and Hamad 2013).

Literature reports revealed the usefulness of response surface methodology (RSM) in studying the interactions of two or more variables that influences adsorption processes (Adetokun et al. 2019; Garba et al. 2019a, b; Jawad et al. 2017; Mohammad et al. 2019). We chose to apply central composite design (CCD) among many subsets of RSM in our work because it is a technique that does not require much experimentation in probing the extent of influence exerted by the parameters to be optimized (Hameed et al. 2009). Another added advantage of CCD is its ability to trim experiments that are inconsequential as well as checkmate the possibility of synergy existing amongst the factors.

Experimental section

Anhydrous $CuSO_4$ and prometryn as adsorbate are the main reagents employed in this work, together with MCC. In the preparation of adsorbate stock solutions, 1 g of Pr was dissolved in 1 L volumetric flask to form 1000 mg/L concentration which was appropriately diluted using de-ionized water. All the analytical grade chemicals used are supplied by Aladdin Industrial Corporation and Shanghai Macklin Biochemical Co ltd Shanghai, China which were used without further purification.

Preparations of Cu-MCC composite

About 1.591 g of anhydrous $CuSO_4$ was dissolved in 100 mL distilled water to produce 0.10 M solution. After dissolving the $CuSO_4$ crystals, 2.5 g of MCC was then introduced into the solution mixture and then homogenized at room temperature for 3 h to achieve complete homogenization. The mixture was then heated under reflux at 80 °C for 5 h to form the composite which was then filtered, washed and dried at 100 °C overnight. The product was washed several times again with de-ionized water to get rid of residual reagents from the mixture and labeled as Cu-MCC. The preparation procedure was depicted in Fig. 1 and explained as follows: Upon introducing Cu^{2+} from copper sulphate onto the hydroxyl containing surface of MCC, electrostatic attraction played a key role in attracting Cu^{2+} onto the MCC surface leading to a distinct coordination with oxygen from the hydroxyl group.

Cu is attached to the MCC by a typical coordination formed between Cu^{2+} and oxygen of hydroxyl or ether group (Hernandez et al. 2007) as depicted in Fig. S1.

Adsorbent characterization

The surface morphology and elemental content of the MCC and Cu-MCC were observed with the aid of a Scanning Electron Microscopy (SEM) and Energy-dispersive X-ray spectrometry (EDS) respectively. The surface area and pore size of the MCC and Cu-MCC composite were analyzed from N_2 physisorption at − 196 °C using Brunauer–Emmett–Teller (BET) equation and Autosorb-iQ analyzer (Quantachrome) equipment. In order to study the X-ray diffraction patterns of MCC and the Cu-MCC composite, X-ray diffractometer (X'Pert PROMRD 3040) was employed for the identification of the phase constitution and crystal structure of the samples. Surface functional groups as well as the surface chemistry of the samples were determined with the aid of FTIR analyses (4000 to 400 cm^{-1}) which was carried out using Nicolet™iS™ 5 spectrometer as well as X-ray photoelectron spectroscopy (XPS, ESCALAB 250 Thermo-VG Scientific) respectively. A method reported by (Islam et al. 2017) was adopted in evaluating the surface charge (pH_{pzc}) of the adsorbent using a pH meter, taking the pH_{pzc} as a value when the final pH is equal to the initial pH. The surface is

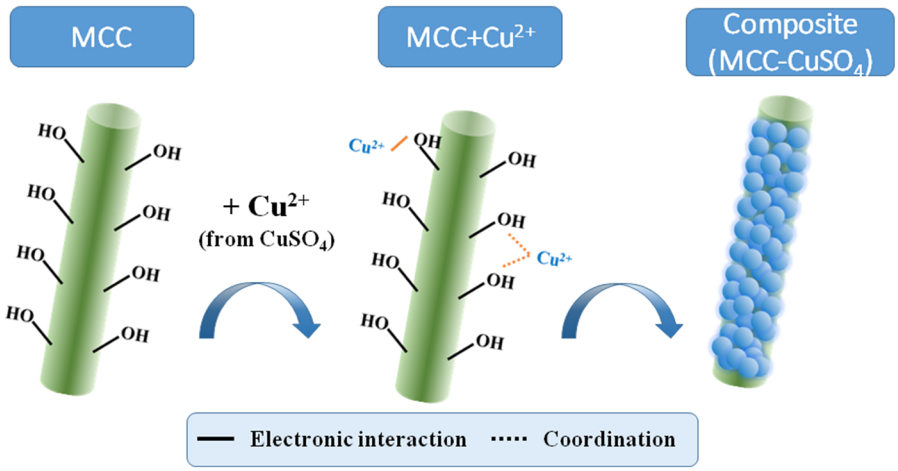

Fig. 1 Schematic diagram of the Cu-MCC composite preparation process

deemed to be neutral, negatively charged or positively charged when $pH = pH_{pzc}$, $pH > pH_{pzc}$ or $pH < pH_{pzc}$ respectively (Babic et al. 1999).

Pr adsorption–desorption experiments

Series of batch adsorption experiments were carried out in a set of 250 mL Erlenmeyer flasks to study and evaluate how the three adsorption variables influences the Pr percentage removal as shown in Table 1. The code given to the variables as well as their range of values were depicted in Table 2. Mechanical shaker was employed for the adsorption which agitated the flasks at different shaking speeds (Table 1). Ultraviolet–Visible (UV 2500) spectrophotometer was used in determining the remaining concentration of the Pr adsorbate. The Pr removal efficiency was evaluated as

$$\text{Pr adsorption efficiency } (\%) = \frac{C_o - C_e}{C_o} \times 100 \quad (1)$$

where C_o and C_e are the initial and equilibrium concentrations (mg/L), respectively.

The equilibrium amount adsorbed q_e(mg/g) was evaluated using Eq. 2:

$$q_e = \frac{(C_o - C_e)V}{W} \quad (2)$$

where the solution volume and adsorbent weight were denoted as V (L) and W (g) respectively.

The adsorbed Pr amount adsorbed at different time intervals q_t (mg/g) was deduced using Eq. 3:

$$q_t = \frac{(C_o - C_t)V}{W} \quad (3)$$

where C_t (mg/L) is the the concentration at a given time t, respectively.

After Pr adsorption, the regeneration of Cu-MCC was carried out by filtering out the adsorbent which was then immersed using 0.02 M HCl with shaking for 3 h. After completing the elution, Cu-MCC was then washed and dried to recover the regenerated adsorbent. The regenerated Cu-MCC was subjected to repeated sequential cycles of the adsorption–desorption.

Adsorption isotherm

The equilibrium data generated was subjected to Langmuir and Freundlich isotherm models. Linear form of Langmuir model is given as (Langmuir 1918):

$$\frac{C_e}{q_e} = \frac{1}{K_L \cdot Q_a^0} + \frac{C_e}{Q_a^0} \quad (4)$$

Q_a^0 (mg/g) and K_L (L/mg) are monolayer adsorption capacity and Langmuir constant respectively. The dimensionless separation factor, R_L, given as:

$$R_L = \frac{1}{1 + K_L C_o} \quad (5)$$

It values give an idea about favorability ($0 < R_L < 1$), unfavorability ($R_L > 1$), linearity

Table 1 Experimental design matrix using central composite design

Run	Level			Prometryn (Pr) adsorption variables			Pr removal
				Adsorbent dosage (g)	pH	Shaking speed (rpm)	Y_{Pr} (%)
1	− 1	− 1	− 1	0.38	4	130	44.16
2	+ 1	− 1	− 1	1.22	4	130	51.78
3	− 1	+ 1	− 1	0.38	12	130	93.48
4	+ 1	+ 1	− 1	1.22	12	130	59.22
5	− 1	− 1	+ 1	0.38	4	220	47.58
6	+ 1	− 1	+ 1	1.22	4	220	35.09
7	− 1	+ 1	+ 1	0.38	12	220	91.23
8	+ 1	+ 1	+ 1	1.22	12	220	73.32
9	− 1.682	0	0	0.1	8	175	73.14
10	+ 1.682	0	0	1.5	8	175	32.84
11	0	− 1.682	0	0.8	2	175	32.52
12	0	+ 1.682	0	0.8	14	175	90.64
13	0	0	− 1.682	0.8	8	100	71.15
14	0	0	+ 1.682	0.8	8	250	89.84
15	0	0	0	0.8	8	175	66.71
16	0	0	0	0.8	8	175	67.11
17	0	0	0	0.8	8	175	68.26
18	0	0	0	0.8	8	175	68.36
19	0	0	0	0.8	8	175	67.78
20	0	0	0	0.8	8	175	69.32

Table 2 Independent variables and their coded levels using central composite design

Variables	Code	Unit	Coded variable levels				
			− α	− 1	0	+ 1	+ α
Adsorbent dosage	x_1	g	0.10	0.38	0.80	1.22	1.50
pH	x_2	–	2	4	8	12	14
Shaking speed	x_3	rpm	100	130	175	220	250

(R_L = 1), and/or irreversibility of an adsorption process (R_L = 0).

The linear form of Freundlich model on the other hand is expressed as (Freundlich 1906):

$$\log q_e = \log K_F + \frac{1}{n}\log C_e \quad (6)$$

K_F and n are Freundlich constants. Generally, $n > 1$ suggests favorable adsorption (Martins et al. 2015).

Design of experiments using response surface methodology (RSM)

CCD, one of the many subsets of RSM was used here to study three factors that influence Pr adsorption. Detailed explanation of the science behind CCD was reported in our previously published papers (Afidah and Garba 2015; Garba and Afidah 2015). The software model employed in this work is design expert statistical software (version 7.0.8 Stat Ease, Inc., Minneapolis, MN 55413, USA).

Results and discussion

Characterization

To compare the surface before and after incorporating Cu^{2+} particles, MCC is presented as control. The changes caused by incorporating Cu^{2+} on the MCC can be seen clearly. The original MCC is white (Fig. 2a), while the color change with respect to the Cu-MCC composite can be clearly observed even at a glance (Fig. 2d). Another important observation from the SEM images is typical features of cellulose fibers informed by the dispersed netting lines and natural piral twists on the MCC surface (Fig. 2b). Other authors also reported similar morphology in their work on MCC (Hamad et al. 2018). At higher magnification from the SEM (Fig. 2c), nanoporous surface can be observed with some microfibrils which provided efficient points that anchor the growth of Cu^{2+} particles.

Some particles (marked by a circle) can be seen dispersed on the Cu-MCC (Fig. 2e, f). These particles show the successful incorporation of Cu^{2+} from $CuSO_4$ on the prepared composite. Typical EDS spectrum of Cu-MCC (Fig. 3) further confirmed the presence of Cu in the composite sample.

The results obtained for BET surface area, cumulative pore volume, and average pore diameter of the MCC and Cu-MCC are given in Table 3. As can be seen, the improvement in the BET surface area from 5.54 m^2/g (MCC) to 6.06 m^2/g (Cu-MCC) was attributed to the presence of active sites on the adsorbent. On the contrary, decrease in the cumulative pore volume from 0.015 cm^3/g (MCC) to 0.010 cm^3/g (Cu-MCC) was ascribed to the incorporated Cu particles on the adsorbent surface which make the Cu-MCC to be dense and compact.

Tan et al. (2018) revealed similar result when they developed an immobilized microcrystalline cellulose and employed it in the adsorption of cationic dye.

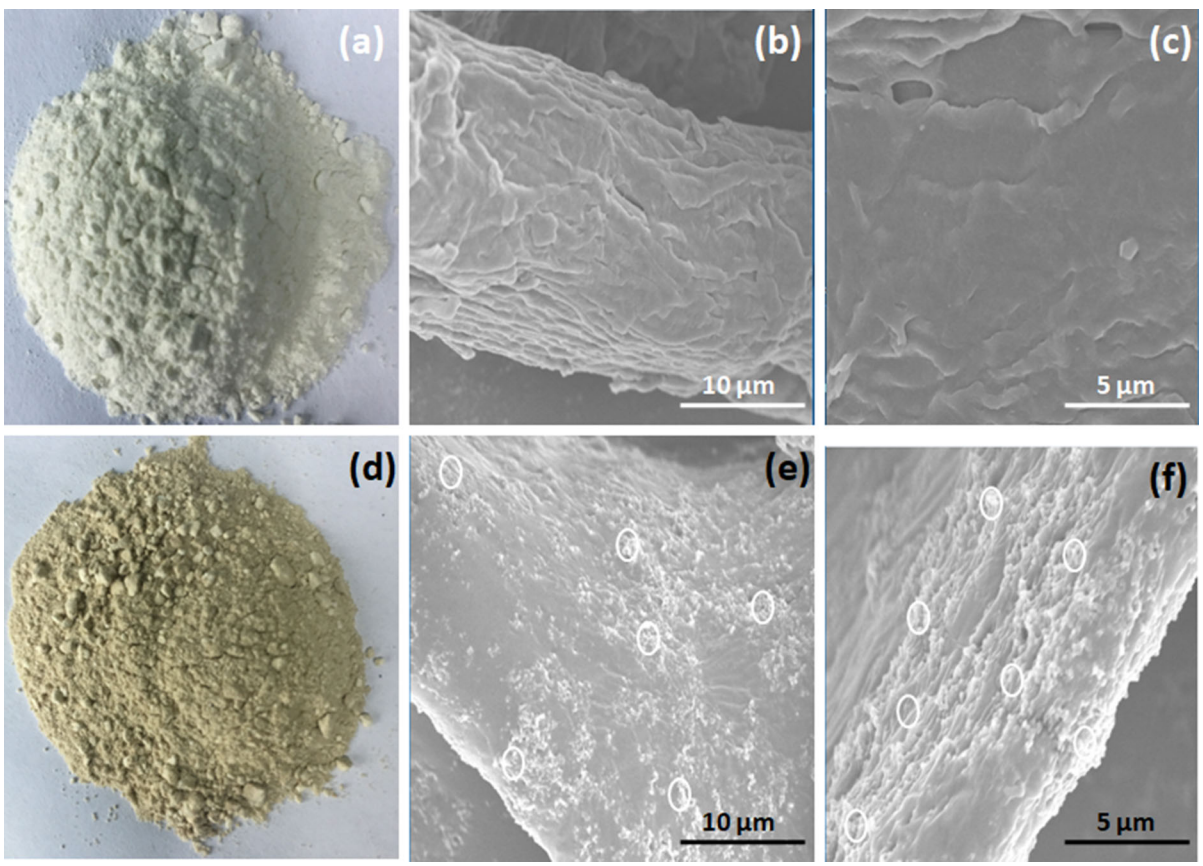

Fig. 2 **a–f** The photographs and SEM images of the MCC and Cu-MCC composite

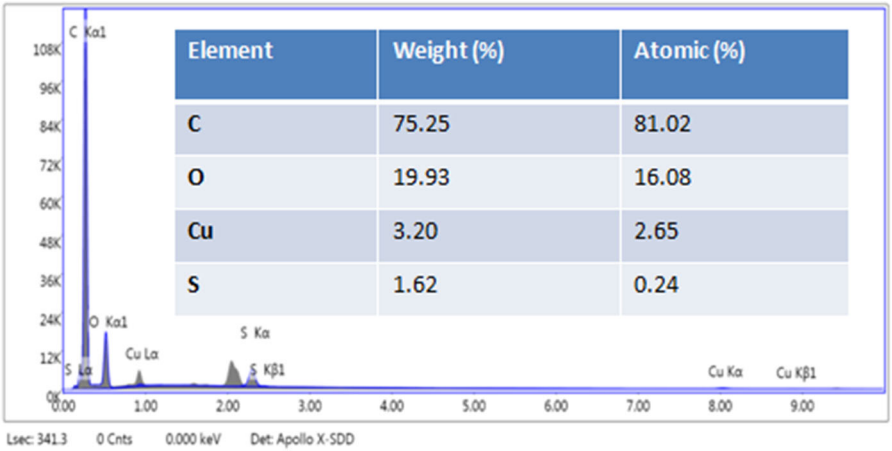

Element	Weight (%)	Atomic (%)
C	75.25	81.02
O	19.93	16.08
Cu	3.20	2.65
S	1.62	0.24

Fig. 3 EDS spectrum and Table (inset) showing the elemental composition of Cu-MCC composite

Table 3 Surface and porosity parameters of MCC and Cu-MCC

Sample	BET surface area (m^2/g)	Cumulative pore volume (cm^3/g)	Average pore width (nm)
MCC	5.54	0.015	10.77
Cu-MCC	6.06	0.010	11.52

They reported an increment in the surface area from 2.04 to 4.95 m^2/g well as a reduction in total pore volume from 0.0070 to 0.0033 cm^3/g of MCC derived from Oil Palm fronds (OPF MCC) to immobilized OPF MCC respectively.

From the average pore diameter value of 11.52, the Cu-MCC adsorbent can be categorized as mesoporous based on IUPAC classification. The IUPAC classified the pores with > 50 nm diameter as macropores, 2–50 nm diameter as mesopores, and < 2 nm diameter as micropores (Tan et al. 2018).

The FTIR spectra depicting the chemical structure of MCC before and after incorporating Cu^{2+} was shown in Fig. 4. The appearance of a vital band related to the metal–oxygen bond vibrations can be seen on the Cu-MCC composite spectra at 541 cm^{-1} which clearly confirmed the presence of a metal ion (Cu^{2+}) in the composite sample. The polymorphs of highly crystalline cellulose are characterized by bands in the region of 1500–800 cm^{-1} (Jiao et al. 2017). From Fig. 4, the IR bands that appeared at 1376 and 862 cm^{-1} were attributed to CH_2 scissoring motion and C–O–C stretching at b-(1–4)-glycosidic linkage.

Those two peaks represented a typical characteristic of crystalline cellulose type I (Jiao et al. 2017). In preparing the Cu-MCC composite, incorporation of Cu^{2+} onto the MCC kept the original MCC structure intact as informed by lack of change of these peaks at 1376 and 862 cm^{-1} suggesting that no chemical changes to MCC occurred. Similar result was reported by other researchers when they incorporated MnO_2 onto MCC which was utilized as adsorbent for Pb^{2+} removal (Jiao et al. 2017). The XRD patterns of MCC and Cu-MCC composite are depicted in Fig. 5a for comparison and confirmation of Cu-MCC composite crystalline properties. The peaks at 2 theta values of 14.78°, 15.98°, 22.24° and 34.48° for MCC were ascribed to (1–10), (110), (200) and (004) crystallographic planes (JCPDS no. 00-050-2241) which agreed with the typical cellulose Iβ diffraction peaks (French 2014; French and Santiago Cintrón 2013; Lu et al. 2014). Upon comparing the peaks on Cu-MCC composite with those peaks on MCC, there were no significant changes observed, confirming that incorporating Cu^{2+} does not alter the MCC crystal structure. This XRD result was in good agreement with the conclusions derived from the FTIR spectra.

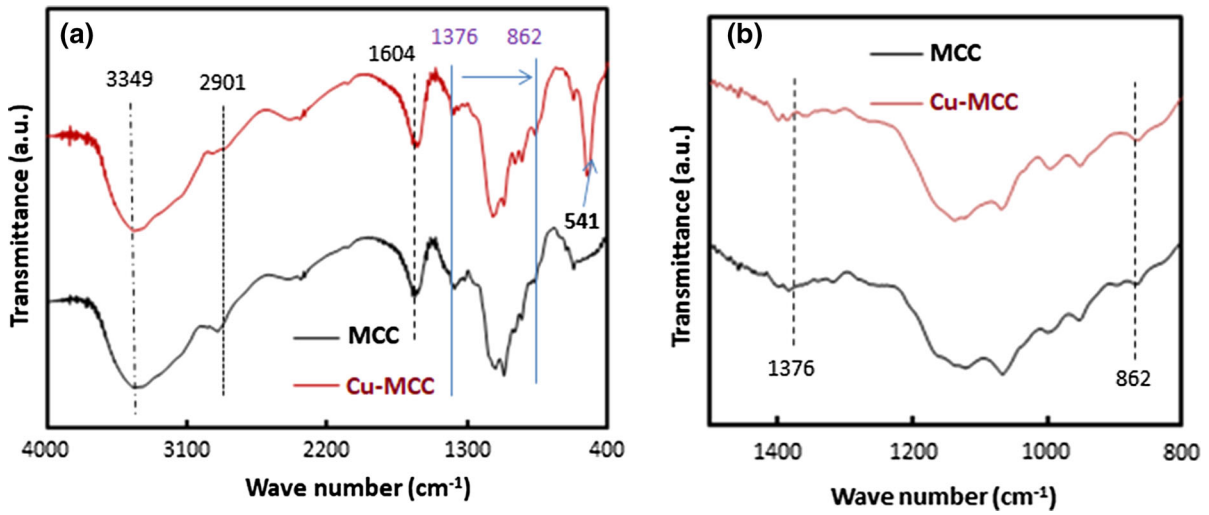

Fig. 4 **a** FTIR spectra and **b** local magnified spectra of MCC and Cu-MCC composite

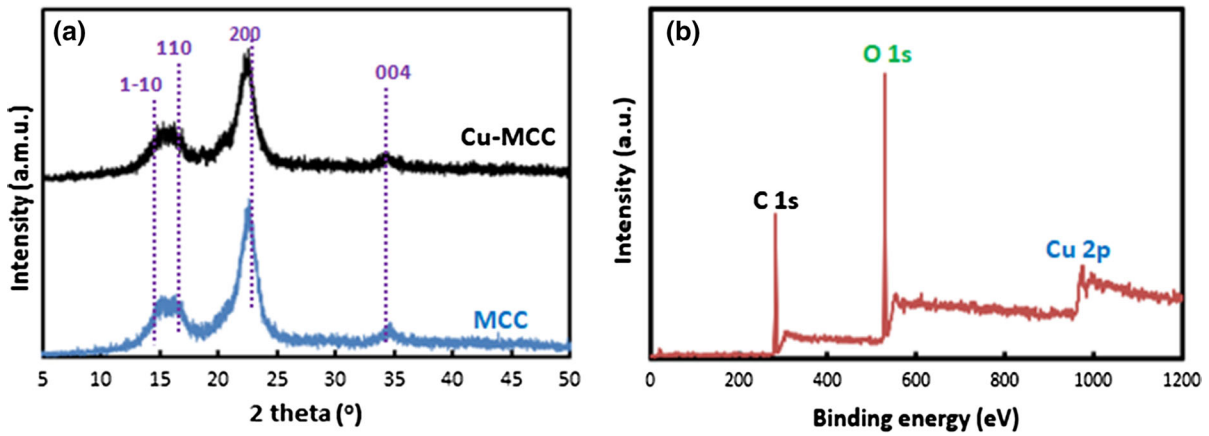

Fig. 5 **a** XRD patterns of MCC and Cu-MCC composite, **b** XPS survey spectra of Cu-MCC composite

To gain further insight into the surface elemental composition and speciation of Cu-MCC, XPS analysis was carried out with the result depicted in Fig. 5b. The peak (951 eV) on the spectra provided further evidence that Cu^{2+} was successfully incorporated onto MCC. The C binding energy of 285 eV was used as reference in evaluating the accompanying elements. Other researchers correlated XPS spectra at 932.4 and 952.3 eV with Cu $2p_{3/2}$ and Cu $2p_{1/2}$ respectively (Aslam et al. 2002). They further reported the presence of Cu zero state based on high-resolution spectrum between 925 and 960 eV. C–C bonds which explain the C 1 s region was associated with the peak at 283 eV. This is in agreement with other researchers who reported the C 1 s region on their samples with binding energies at 284.1 and 285.3 eV to be associated with C–C bonds and C–O or C–OH bonds respectively (Božič et al. 2014; Hamad et al. 2018). Another peak at 529 eV explained the O 1 s region in the Cu-MCC sample. Other researchers also reported peaks for O 1 s region at similar binding energy values of 531.9 and 530 eV to be associated with C–OH groups and O–C–O bonds respectively (Hamad et al. 2018).

Pr adsorption study

A preliminary adsorption study was carried out with the aim of comparing the MCC and Cu-MCC using various $CuSO_4$ concentrations so as to evaluate how

Cu^{2+} incorporation onto the MCC improved its adsorption capability. As shown in Fig. S2, there was an upsurge in the amount of Pr taken up with raise in the concentration of $CuSO_4$ (0 to 0.10 M), after which it almost plateaud despite further increase in the concentration, hence subsequent Pr adsorption studies were done with the Cu-MCC composite prepared using 0.10 M $CuSO_4$ concentration.

Development of regression model equations using CCD

The experimental design comprising the Pr adsorption variables and the response (Y_{Pr}) were displayed in Table 1. Some preliminary experiments and literature guided our choice of the adsorption variables and their ranges as shown in Table 2. The Pr percentage removal values ranged from 32.52 to 93.48% (Table 1). The software chose quadratic as the most suitable model which was applied for the response (Pr removal). The experimental error and reproducibility of the data were determined by the six replicate variables at the center points (run 15–20). Upon correlation using CCD, the polynomial regression equation developed for the response was a quadratic expression as suggested by the software. The highest order of polynomial, model not aliased as well as the significance of additional terms guided the selection of model expression. The predicted and experimental data (Fig. 6a) show good correlation based on the model's R^2 value of 0.9446 which agreed well with adjusted R^2 (Adj. R^2) value of 0.8948. The R^2 value of 0.9446 also implied that the total variation that cannot be explained by the model constitutes only 5.54%. The model equation generated for Y_{Pr} response is given as:

$$\begin{aligned} Y_{Pr} = {} & 68.01 - 9 - 14x_1 + 17.31x_2 + 2.20x_3 \\ & - 5.91x_1x_2 - 0.47x_1x_3 + 3.14x_2x_3 - 5.88x_1^2 \\ & - 2.85x_2^2 + 3.84x_3^2 \end{aligned} \quad (7)$$

The positive and negative signs in the equation depict synergetic and antagonistic effects of the respective variables respectively (Garba and Afidah 2014). The single variables, two variables and second order term of variables signified a uni-factor, double factor and quadratic effects respectively (Ahmad and Alrozi 2010a).

Statistical analysis

The ANOVA generated for the surface quadratic model in the percentage removal of Pr was presented on Table 4. ANOVA is very crucial in validating the significance and adequacy of the model. The mean square values on the table were calculated when the sum of squares of each of the variation sources and the error variance were divided by the acquired degrees of freedom (Ahmad and Alrozi 2010b). If Prob. > F value is less than 0.05 for a particular term, it show that the term from the model is significant.

The model F-value of 18.96 and Prob. > F of < 0.0001 signified the model's significance. The significant model terms were $x_{1,}x_2, x_1x_2, x_1^2$ and x_3^2. The remaining terms x_3, x_1x_3, x_2x_3 and x_2^2 had little significance to the response. It can be deduced that, within the range of the studied variables, the model is very suitable in predicting Pr removal.

Adequate precision (AP) is the parameter used in gauging the signal to noise ratio with a value above 4 depicting appropriateness. In this case, an adequate signal was signified for Y_{Pr} based on the ratio value of 16.08 which infers that the design space can be steered by this model.

To provide more usable information on the model's suitability, the residuals (difference between the experimental and the predicted response values) were analyzed. This analysis is crucial in identifying the outliers as well as examining the diagnostic (normal probability and residual) plots. If the normal probability plot of a residual follows normal distribution, then the points will form a straight line (Alidokht et al. 2011). Figure 6b shows the normal probability plot of the residual for Pr removal. The plot resembles a straight-line graph showing that the residual is normally distributed with the trend revealing a reasonably well-behaved residual for the Pr herbicide. Additionally, Fig. 6c revealed the residual vs. predicted response plot. The assumption of constant variance was tested by the plot showing the residual versus the ascending predicted response. Randomly scattered points can be observed on the plot (Fig. 6c) with a constant range of residuals across the graph, demonstrating the random fluctuation of residuals in the plot around the center line.

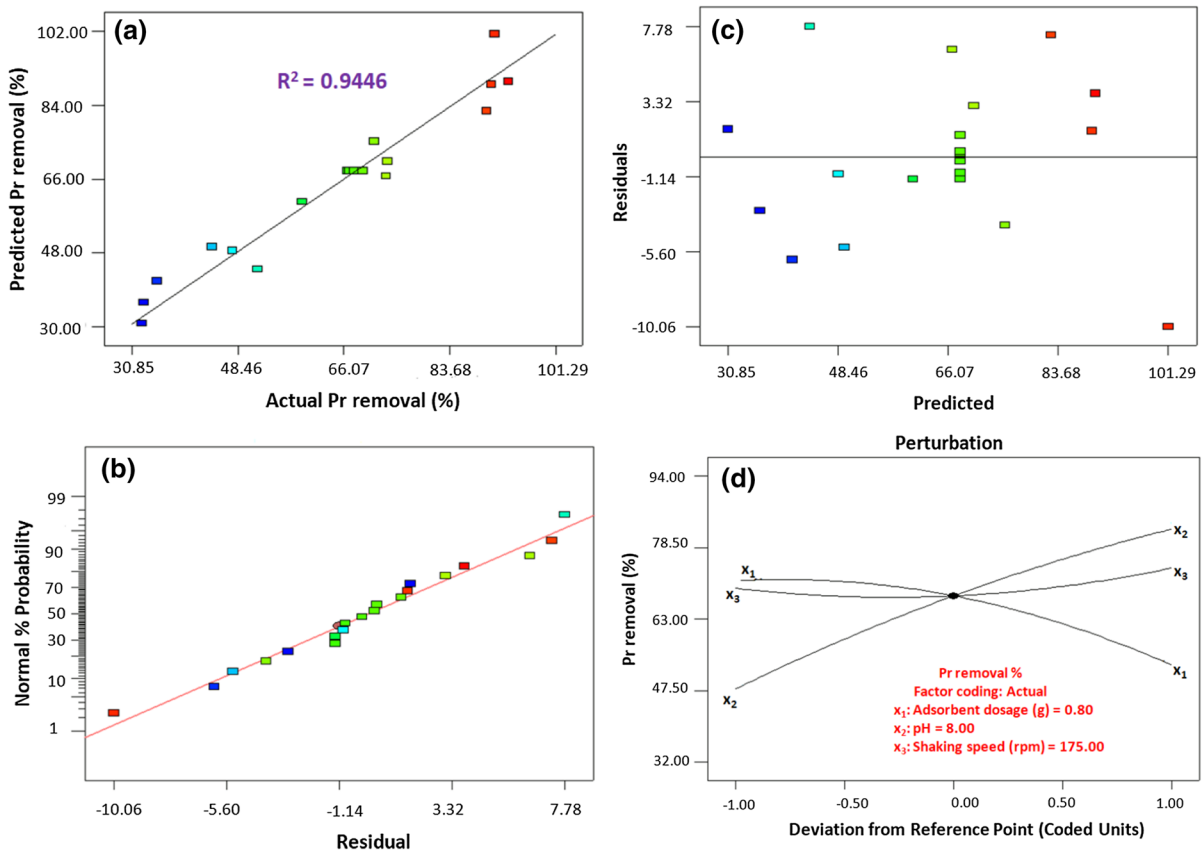

Fig. 6 **a** Comparison of the actual results with the predicted values, **b** Normal probability plots, **c** Residual versus predicted response values and **d** Perturbation plots for Pr removal efficiency onto Cu-MCC composite

Table 4 The ANOVA for response surface quadratic model of Pr adsorption onto Cu-MCC

Source	Sum of squares	Degree of freedom	Mean square	F value	Prob > F
Pr					
Model	6546.51	9	727.39	18.96	< 0.0001
x_1	1140.75	1	1140.75	29.73	0.0003
x_2	4091.59	1	4091.59	106.63	< 0.0001
x_3	65.96	1	65.96	1.73	0.2191
x_1x_2	279.66	1	279.66	7.29	0.0223
x_1x_3	1.77	1	1.77	0.05	0.8344
x_2x_3	78.88	1	78.88	2.06	0.1822
x_1^2	498.93	1	498.93	13.00	0.0048
x_2^2	116.80	1	116.80	3.04	0.1116
x_3^2	212.57	1	212.57	5.54	0.0404
Residual	383.71	10	38.37	–	–
A.P. 16.08		R^2 0.9446		Adj. R^2 0.8948	

Individual, interaction and quadratic effects of the variables

The large F-values of 106.63 and 29.73 for solution pH and adsorbent dosage respectively (Table 4) depicts that they inflicted higher individual effects on Pr percentage removal and both were significant whereas the effect of shaking speed was smaller on this response showing F-value of 1.73. To enquire more on the individual effect of the three independent variables (adsorbent dosage coded as x_1, solution pH coded as x_2 and shaking speed coded as x_3) on the response (Pr removal), perturbation plots were employed. In perturbation plot, the influence of a particular model term is shown by deviating it from the reference point on the response, with other factors kept constant. The software automatically set the reference point at the midpoint (coded 0) for all the factors, and then the most significant factor on the response was probed with the aid of the perturbation plot. The sensitivity of a response to a particular variable is informed by a steep slope or curvature while the insensitivity to change of the response with respect to that particular variable is indicated by a relatively flat line (Jawad et al. 2015). With respect to Pr removal efficiency, the perturbation plots are shown in Fig. 6d. The response sensitivity to all the factors studied can be seen by forming a sharp curvature for all the independent variables. An upsurge in the Pr removal can also be noticed after an increase in adsorbent dosage (factor x_1) and pH (factor x_2). Meanwhile, there was slight increase in the Pr removal with decrease in the shaking speed (factor x_3). There was also a significant interaction between pH and adsorbent dosage based on the F-value of 7.29 (Table 4). However, interaction between other factors were insignificant based on their F and Prob > F values.

The interaction terms of x_1x_2 on the response were depicted on Fig. 7 in the form of 3D and contour plots. A simultaneous increase in the adsorbent dosage and solution pH leads to an upsurge in Pr removal efficiency. The ability of Cu-MCC adsorbent to remove Pr molecules from a given solution was informed by adsorbent dosage with the solution pH responsible for the surface charge; hence the big influence of their interaction on the model. The competition between H_3O^+ and Pr cations for the adsorption sites explain the low Pr removal at acidic solution.

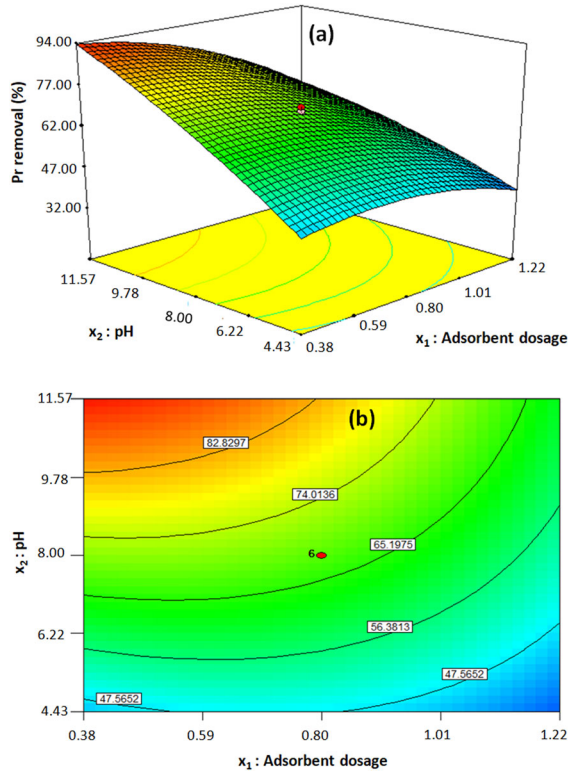

Fig. 7 **a** 3-D response surface and **b** contour plots of the Pr removal efficiency as the function of pH and adsorbent dosage (shaking speed = 175 rpm)

The quadratic effects of adsorbent dosage and shaking speed were more pronounced with F-values of 13.00 and 5.54 respectively while that of solution pH was low and insignificant with F-value of 3.04.

Confirmation experiment

The identified optimum predicted conditions were adsorbent dosage of 0.40 g, solution pH of 11 and shaking speed of 215 rpm giving rise to the predicted and experimental Pr removal (response) values of 97.68 and 98.46% respectively (Table 5). This observation indicates less deviation between predicted and experimental Pr removal values. For all the ensuing studies, the given optimal results (adsorbent dosage of 0.40 g, solution pH of 11 and shaking speed of 215 rpm) were chosen and used.

Solution pH is a crucial factor that influenced the Pr adsorption mechanism. Protonation of Pr molecule at low pH (strongly acidic) solution occurred according to Fig. S3a with resonance effect playing a key role in

Table 5 The CCD for three independent variables with predicted and experimental responses (Pr removal %)

Model desirability	Adsorbent dosage, x_1 (g)	pH, x_2	Shaking speed, x_3 (rpm)	Pr removal (%)		
				Predicted	Experimental	Error
1.00	0.40	11	215	97.68	98.46	0.79

stabilizing the protonated molecule (Grabka et al. 2015). In acidic solutions (low pH), only protonated molecules are present but on raising the pH above 7, the basic solution contain mainly neutral molecules (Grabka et al. 2015). Thus, π–electron interactions can be held responsible for the Pr adsorption in alkaline solution. The pHpzc value of the Cu-MCC was determined from Fig. S3b to be 11.3 which is almost the same as the optimum solution pH of 11 as determined by the software. This observation depicted the neutral character of the composite as well as reconfirming the availability of the neutral Pr molecules which were held on the Cu-MCC surface by π–electron interactions.

Equilibrium and kinetic modelling

Langmuir and Freundlich isotherm equations were plotted to dissect the equilibrium data and also determine the best fitted model for the adsorption of Pr with the respective plots depicted in Fig. 8a, b.

The isotherm parameters (Q_a^0, K_L, R_L, K_F, n) together with R^2 values obtained from Fig. 8a, b are compiled in Table 6. The maximum adsorption capacities for Pr removal by Cu-MCC were 97.80, 116.79 and 119.70 mg/g at 303, 313 and 323 K respectively. Compared with modified halloysite adsorbent reported from literature for Pr adsorption (Grabka et al. 2015), Cu-MCC shows improved adsorption. Therefore, putting into consideration the environmentally friendly design aspect, Cu^{2+} incorporation onto MCC can be said to be successful in producing a promising adsorbent material for the treatment of wastewater contaminated with Pr. Meanwhile, n values (2.418–3.388) depicted from the Freundlich isotherm model are greater than unity, confirming its suitability as good adsorbent for the removal of Pr at all temperatures. Still from Table 6, the amounts of Pr taken up by Cu-MCC were best suited to be described by the Langmuir isotherm

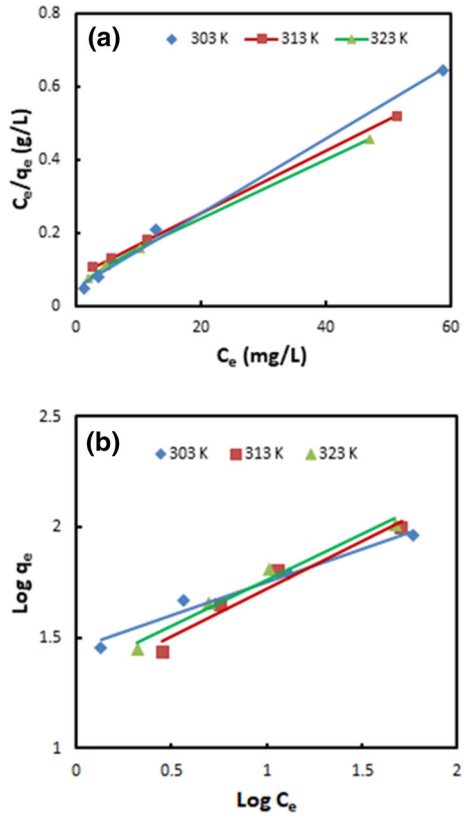

Fig. 8 **a** Langmuir adsorption isotherm plots and **b** Freundlich adsorption isotherm plots for Pr adsorption onto Cu-MCC

model, with high R^2 (0.9953–0.9999) indicating that Pr adsorption occurred at a homogeneous Cu-MCC surface.

Comparison was made with various adsorbents from literature for the adsorption of herbicides, as compiled in Table 7. From this table, we conclude Cu-MCC to have the potentials of being a good adsorbent material for the adsorption of Pr herbicide from wastewater.

The pollutant adsorption rate can be depicted with the aid of adsorption kinetics. According to Fig. 9a, there was an upsurge in the adsorption rate for the first

Table 6 Isotherm parameter constants for Pr adsorption onto Cu-MCC at different temperatures

Isotherm temperature (K)	Langmuir isotherm				Freundlich isotherm		
	Q_a^0 (mg/g)	K_L (L/mg)	R_L	R^2	K_F ($mg^{1-n}/g\ L^n$)	n	R^2
303	97.80	0.210	0.031	0.9953	28.510	3.388	0.9737
313	116.79	0.106	0.059	0.9999	19.498	2.315	0.9532
323	119.70	0.127	0.050	0.9987	22.305	2.418	0.9745

Table 7 Comparison of Cu-MCC with various adsorbents for the adsorption of herbicides from synthetic water at room temperature

Adsorbent	Adsorbate	Q_a^0 (mg/g)	References
Cu-MCC	Prometryn	97.80	This work
Modified halloysite	Prometryn	0.50	Grabka et al. (2015)
Commercial activated carbon	Carbofuran	96.15	Salman and Hameed (2010a)
Bagasse fly ash	2,4 Dichloro-phenoxyacetic acid	5.63	Deokar et al. (2016)
Cladium mariscus	2,4-Dichlorophenoxyacetic acid	65.58	Bartczak et al. (2016)
Apple shell	Chlorophenoxy acid	28.50	Okumus et al. (2015)
Orange peel	Chlorophenoxy acid	137.04	Okumus et al. (2015)
Banana peel	Chlorophenoxy acid	2.39	Okumus et al. (2015)
Millet waste	Chlorophenoxy acid	156.3	Okumus et al. (2015)

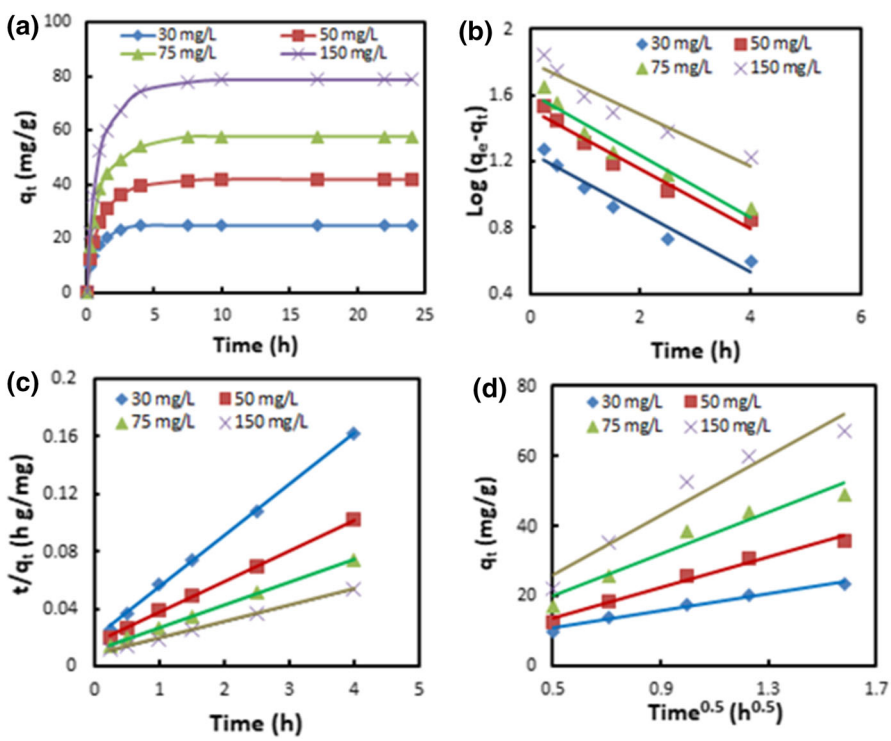

Fig. 9 **a** Adsorption behavior of Cu-MCC composite at various initial concentrations, **b** pseudo-first-order kinetic plots, **c** pseudo-second-order kinetic plots and **d** Intraparticle diffusion plots for Pr adsorption

3 h, then began to slow down gradually to about 5 h before it leveled off for all initial concentrations (30–150 mg/L). For more insight knowledge on the nature of Pr adsorption onto Cu-MCC, the adsorption data generated were fitted by the pseudo-first-order, pseudo-second-order and intra-particle diffusion kinetic model with their respective equations expressed as:

$$\log(q_e - q_t) = \log q_e - \frac{k_1}{2.303} t \quad (8)$$

$$\frac{t}{q_t} = \frac{1}{k_2 q_e^2} + \frac{1}{q_e} t \quad (9)$$

$$q_t = k_{pi} t^{0.5} + C \quad (10)$$

where q_e and q_t are the amounts of Pr adsorbed (mg/g) at equilibrium and at time t (h), respectively while k_1 (1/h) and k_2 (g/mg h) are the adsorption rate constants of pseudo first and second-order adsorption respectively, k_{ip} is rate constant of the intra-particle diffusion equation and C gives information about the boundary layer thickness: larger value of C is associated with the boundary layer diffusion effect. Figure 9b–d shows the fitting curves for the models from where the kinetic parameters presented in Table 8 were evaluated. There was an inconsistent trend in the R^2 values obtained for the pseudo-first-order model with poor or no good agreement between experimental (q_{eexp}) and the calculated (q_{ecal}) values obtained from the linear plots (Fig. 9b). This shows poor fitting of the Pr kinetic adsorption data with pseudo first-order model. On the contrary, the closeness of obtained R^2 values to unity indicated that the kinetic adsorption data obeyed pseudo-second-order model. A good agreement between q_{eexp} and q_{ecal} values further confirmed the suitability of pseudo-second-order as the best model in describing the kinetics data of Pr adsorption.

Additionally, different adsorbate concentrations lead to the multi-linear plots on Fig. 9d which connotes the simultaneous occurrence of both surface adsorption and intra-particle diffusion during the process (Ren et al. 2011). The values of k_{pi}, C_i and R^2 obtained from the plots are given in Table 9. An increase in the values of k_p and C for Pr adsorption onto Cu-MCC after raising initial concentration is related to the increase in the thickness of the boundary layer as well as greater driving force.

Table 8 Pseudo-first-order and pseudo-second-order equation constants at different initial concentrations for Pr adsorption onto Cu-MCC at room temperature

Adsorbent	C_o (mg/L)	q_{eexp} (mg/g)	Pseudo-first-order kinetic model			Pseudo-second-order kinetic model		
			k_1 (1/h)	q_{ecal} (mg/g)	R^2	k_2 (g/mg h)	q_{ecal} (mg/g)	R^2
Cu-MCC	30	28.656	0.415	17.865	0.9495	0.067	27.933	0.9990
	50	46.315	0.416	32.915	0.9642	0.029	46.512	0.9992
	75	62.048	0.436	41.716	0.9450	0.024	62.893	0.9994
	150	91.215	0.340	63.154	0.9291	0.0157	87.719	0.9990

Table 9 Intraparticle diffusion equation constants at different initial concentrations for Pr adsorption onto Cu-MCC at room temperature

Adsorbents	C_o (mg/L)	k_p (mg/g $h^{1/2}$)	C	R^2
Cu-MCC	30	12.393	4.438	0.976
	50	21.897	2.700	0.9791
	75	30.004	4.777	0.9443
	150	42.326	4.900	0.9440

Adsorption thermodynamics

Thermodynamics of the Pr adsorption process were appraised at 30, 40 and 50 °C in order to have an idea about the process spontaneity. The three thermodynamic parameters considered were standard Gibb's free energy (ΔG°), enthalpy (ΔH°) and entropy (ΔS°)

changes which were evaluated with the aid of Van't Hoff equation.

$$\ln K_D = \frac{\Delta S^\circ}{R} - \frac{\Delta H^\circ}{RT} \quad (11)$$

where R (8.314 J/mol/K) is the universal gas constant; T (K) is the absolute temperature; $K_D = \frac{q_e}{C_e}$ which is the distribution coefficient. A linear plot of ln K_D against $\frac{1}{T}$ gives a graph (Fig. S4) with slope and intercept used in computing the ΔH° and ΔS° respectively. ΔG° was calculated using the relation below:

$$\Delta G^\circ = -RT \ln K_D \quad (12)$$

The negative ΔG° values obtained (Table 10) signified feasible and spontaneous process for the Cu-MCC adsorbent in the studied ranges of temperatures. Furthermore, the value of ΔG° indicate whether the process is physical (− 20 to 0 kJ/mol) or chemical (− 80 to − 400 kJ/mol) adsorption. From the values obtained, it can be inferred that the nature of adsorption here is physical (physisorption) with all the values for different temperatures at varying initial concentrations ranging from -1.11 to -7.71 kJ/mol.

The positive ΔH° values obtained indicated an endothermic adsorption process signifying an increase in the amount of Pr adsorbed increased with upon raising the solution temperature. The endothermic nature of this process may be related to stripping of solvating water molecules during adsorption (Jiao et al. 2017) because the exothermic heat produced by the attachment of Pr to the Cu-MCC surface was presumably exceeded by this energy demanding dehydration (Pelosi et al. 2014). ΔS° values obtained for the Pr adsorption process were also presented in Table 10 implying that there was an affinity between Pr and the adsorbent as a result of increasing randomness at Cu-MCC/Pr solution interface as well as an upsurge in the degree of freedom.

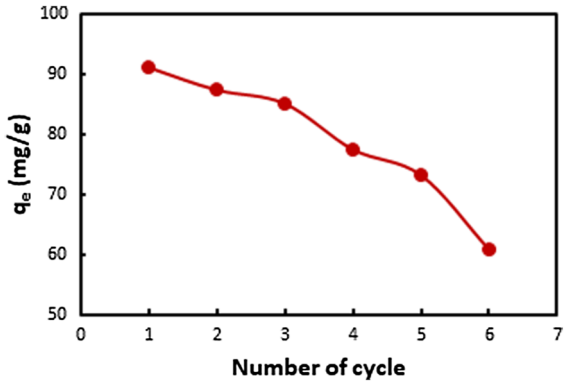

Fig. 10 Adsorption capacity of regenerated Cu-MCC at different number of cycles

Desorption and regeneration studies

Regeneration of an adsorbent is a vital factor for sustainable applications. The ability of Cu-MCC to be regenerated at different number of cycles was shown in Fig. 10.

The sustainability and benign nature of the Cu-MCC was further demonstrated by the slight decrease in the adsorption capacity value of the regenerated adsorbent during six sequential adsorption–desorption cycles (Fig. 10), with the q_e value still about 66.7% of its initial value after regeneration.

Conclusions

A facile synthesis method which involved incorporating Cu^{2+} onto MCC was used efficiently to produce a composite material for the adsorption of Pr herbicide from synthetic wastewater. The method was proved to be better in terms of feasibility, cost-effectiveness and

Table 10 Thermodynamic parameters for the adsorption of Pr onto Cu-MCC at different temperatures and varying initial concentrations (30–150 mg/L)

Adsorbate	C_o (mg/L)	ΔH° (J/mol)	ΔS° (J/mol K)	ΔG° (kJ/mol)		
				30 °C	40 °C	50 °C
	30	− 19.67	− 40.97	− 7.71	− 5.87	− 6.95
	50	− 13.13	− 23.14	− 6.38	− 5.34	− 5.95
Pr	75	11.18	49.93	− 3.95	− 4.46	− 4.94
	150	13.96	49.81	− 1.11	− 1.70	− 2.10

eco-friendliness when compared with the conventional methods which are associated with being complicated, time-consuming and high-temperature. The new composite material in our work was characterized by a range of techniques and the adsorption process was optimized with the aid of a CCD statistical technique. The optimized variables gave rise to the predicted and experimental percentage Pr removal of 97.68 and 98.46% respectively. Textural characterization revealed the Cu-MCC composite to be uniformly coated with birnessite-copper particles. Regeneration study demonstrated the adsorption capacity to be about 66.7% of its initial value after six sequential adsorption–desorption cycles. These results indicate the newness, efficiency and renewability of the Cu-MCC composite with respect to the Pr removal from wastewater.

Acknowledgments The authors would like to humbly acknowledge the international funding provided by Fujian Agriculture and Forestry University (KXB16001A) PR China.

Compliance with ethical standards

Conflict of interest The authors have no conflict of interest with regards to the submission and publication of this article.

References

Adetokun AA, Uba S, Garba ZN (2019) Optimization of adsorption of metal ions from a ternary aqueous solution with activated carbon from *Acacia senegal* (L.) Willd pods using Central Composite Design. J King Saud Univ Sci. https://doi.org/10.1016/j.jksus.2018.1012.1007

Afidah A, Garba ZN (2015) Optimization of preparation conditions for activated carbon from Prosopis africana seed hulls using response surface methodology. Desalin Water Treat 57:17985–17994

Ahmad MA, Alrozi R (2010a) Optimization of preparation conditions for mangosteen peel-based activated carbons for the removal of Remazol Brilliant Blue R using response surface methodology. Chem Eng J 165:883–890

Ahmad MA, Alrozi R (2010b) Removal of Malachite Green dye from aqueous solution using rambutan peel-based activated carbon: equilibrium, kinetic and thermodynamic studies. Chem Eng J 171:510–516

Akçay G, Akçay M, Yurdakoç K (2005) Removal of 2,4-dichlorophenoxyacetic acid from aqueous solutions by partially characterized organophilic sepiolite: thermodynamic and kinetic calculations. J Colloid Interface Sci 281:27–32

Akçay G, Akçay M, Yurdakoç K (2006) The characterization of prepared organomontmorillonite (DEDMAM) and sorption of phenoxyalkanoic acid herbicides from aqueous solution. J Colloid Interface Sci 296:428–433

Alidadi H, Dolatabadi M, Davoudi M, Barjasteh-Askari F, Jamali-Behnam F, Hosseinzadeh A (2018) Enhanced removal of tetracycline using modified sawdust: optimization, isotherm, kinetics, and regeneration studies. Proc Saf Environ Prot 117:51–60

Alidokht L, Khataee AR, Reyhanitabar A, Oustan S (2011) Cr(VI) immobilization process in a Cr-spiked soil by zerovalent iron nanoparticles: optimization using response surface methodology. CLEAN Soil Air Water 39:633–640

Alizadeh N, Shariati S, Besharati N (2017) Adsorption of Crystal Violet and Methylene Blue on azolla and fig leaves modified with magnetite iron oxide nanoparticles. Int J Environ Res 11:197–206

Aslam M, Gopakumar G, Shoba TL, Mulla IS, Vijayamohanan K, Kulkarni SK, Urban J, Vogel W (2002) Formation of Cu and Cu_2O nanoparticles by variation of the surface ligand: preparation, structure, and insulating-to-metallic transition. J Colloid Interface Sci 255:79–90

Ayranci E, Hoda N (2005) Adsorption kinetics and isotherms of pesticides onto activated carbon-cloth. Chemosphere 60:1600–1607

Babic BM, Milonjic SK, Polovina MJ, Kaludierovic BV (1999) Point of zero charge and intrinsic equilibrium constants of activated carbon cloth. Carbon 37:477–481

Bartczak P, Żółtowska S, Norman M, Klapiszewski L, Zdarta J, Komosa A, Kitowski I, Ciesielczyk F, Jesionowski T (2016) Saw-sedge *Cladium mariscus* as a functional low-cost adsorbent for effective removal of 2,4-dichlorophenoxyacetic acid from aqueous systems. Adsorption 22:517–529

Bazrchi S, Bahram M, Nouri S (2018) Equilibrium and kinetic studies on the removal of acid red-14 from aqueous solutions using PSMA. Iran J Sci Technol Trans Sci 42:203–208

Bouamra F, Drouiche N, Abdi N, Grib H, Mameri N, Lounici H (2018) Removal of phosphate from wastewater by adsorption on marble waste: effect of process parameters and kinetic modeling. Int J Environ Res 12:13–27

Božič M, Liu P, Mathew AP, Kokol V (2014) Enzymatic phosphorylation of cellulose nanofibers to new highly-ions adsorbing, flame-retardant and hydroxyapatite-growth induced natural nanoparticles. Cellulose 21:2713–2726

Brillas E, Boye B, Baños MA, Calpe JC, Garrido JA (2003) Electrochemical degradation of chlorophenoxy and chlorobenzoic herbicides in acidic aqueous medium by theperoxi-coagulation method. Chemosphere 51:227–235

Brogan WR III, Relyea RA (2013) Mitigating with macrophytes: submersed plants reduce the toxicity of pesticide-contaminated water to zooplankton. Environ Toxicol Chem 32:699–707

Chuluun B, Iamchaturapatr J, Rhee JS (2009) Phytoremediation of organophosphorus and organochlorine pesticides by *Acorus gramineus*. Environ Eng Res 14:226–236

Das K, Ray D, Bandyopadhyay NR, Sengupta S (2010) Study of the properties of microcrystalline cellulose particles from different renewable resources by XRD, FTIR, nanoindentation, TGA and SEM. J Polym Environ 18:355–363

Deokar SK, Mandavgane SA, Kulkarni BD (2016) Adsorptive removal of 2,4 dichloro-phenoxyacetic acid from aqueous

solution using bagasse fly ash as an adsorbent in batch and packed-bed techniques. Clean Technol Environ Policy 18:1971–1983

Fahma F, Iwamoto S, Hori N, Iwata T, Takemura A (2010) Isolation, preparation, and characterization of nanofibers from oil palm empty-fruit-bunch (OPEFB). Cellulose 17:977–985

French AD (2014) Idealized powder diffraction patterns for cellulose polymorphs. Cellulose 21:885–896

French AD, Santiago Cintrón M (2013) Cellulose polymorphy, crystallite size, and the Segal crystallinity index. Cellulose 20:583–588

Freundlich HMF (1906) Over the adsorption in solution. J Phys Chem 57:385–470

Garba ZN, Afidah AR (2014) Process optimization of $K_2C_2O_4$-activated carbon from Prosopis africana seed hulls using response surface methodology. J Anal Appl Pyrol 107:306–312

Garba ZN, Afidah AR (2015) Optimization of activated carbon preparation conditions from Prosopis africana seed hulls for the removal of 2,4,6-trichlorophenol from aqueous solution. Desalin. Water Treat 56:2879–2889

Garba ZN, Afidah AR (2016) Evaluation of optimal activated carbon from an agricultural waste for the removal of para-chlorophenol and 2,4-dichlorophenol. Proc Saf Environ Prot 102:54–63

Garba ZN, Afidah AR, Bello BZ (2015) Optimization of preparation conditions for activated carbon from Brachystegia eurycoma seed hulls: a new precursor using central composite design. J Environ Chem Eng 3:2892–2899

Garba ZN, Bello I, Galadima A, Aisha YL (2016a) Optimization of adsorption conditions using central composite design for the removal of copper (II) and lead (II) by defatted papaya seed. Karbala Int J Mod Sci 2:20–28

Garba ZN, Ugbaga NI, Amina KA (2016b) Evaluation of optimum adsorption conditions for Ni(II) and Cd(II) removal from aqueous solution by modified plantain peels (MPP). Beni Suef Univ J Basic Appl Sci 5:170–179

Garba ZN, Hussin MH, Galadima A, Lawan I (2019) Potentials of *Canarium schweinfurthii* seed shell as a novel precursor for CH_3COOK activated carbon: statistical optimization, equilibrium and kinetic studies. Appl Water Sci 9:1–13

Grabka D, Raczyńska-Żak M, Czech K, Słomkiewicz PM, Jóźwiak MA (2015) Modified halloysite as an adsorbent for prometryn from aqueous solutions. Appl Clay Sci 114:321–329

Gunny AAN, Arbain D, Jamal P (2017) Effect of structural changes of lignocelluloses material upon pre-treatment using green solvents. In: AIP conference proceedings. https://doi.org/10.1063/1061.4981844

Gurnani V, Singh AK (2004) Equilibrium studies on the optimization of solid-phase extraction of metal ions with pyrogallol-anchored cellulose synthesized by a new method and applications of the extraction in metal enrichment, removal and determination. Ind Eng Chem Res 43:2302–2309

Hamad H, Bailón-García E, Morales-Torres S, Carrasco-Marín F, Pérez-Cadenas AF, Maldonado-Hódar FJ (2018) Physicochemical properties of new cellulose-TiO_2 composites for the removal of water pollutants: developing specific interactions and performances by cellulose functionalization. J Environ Chem Eng 6:5032–5041

Hameed BH, Tan IA, Ahmad AL (2009) Preparation of oil palm empty fruit bunch-based activated carbon for removal of 2,4,6-trichlorophenol: optimization using response surface methodology. J Hazard Mater 164:1316–1324

Hashem A, El-Shishtawy RM (2001) Preparation and characterization of cationized cellulose for the removal of anionic dyes. Adsorp Sci Technol 19:197–210

Hernandez RB, Yola OR, Merce ALR (2007) Chemical equilibrium in the complexation of first transition series divalent cations Cu^{2+}, Mn^{2+} and Zn^{2+} with chitosan. J Braz Chem Soc 18:1388–1396

Hladik ML, Roberts AL, Bouwer EJ (2005) Removal of neutral chloroacetamide herbicide degradates during simulated unit processes for drinking water treatment. Water Resour 39:5033–5044

Hu D, Wang P, Li J, Wang L (2014) Functionalization of microcrystalline cellulose with *n*,*n*-dimethyldodecylamine for the removal of Congo Red dye from an aqueous solution. BioResources 9:5951–5962

Hussin MH, Pohan NA, Garba ZN, Kassim MJ, Afidah AR, Brosse N, Yemloul M, Fazita MRN, Haafiz MKM (2016) Physicochemical of microcrystalline cellulose from oil palm fronds aspotential methylene blue adsorbents. Int J Biol Macromol 92:11–19

Islam MA, Sabar S, Benhouria A, Khanday WA, Asif M, Hameed BH (2017) Nanoporous activated carbon prepared from karanj (*Pongamia pinnata*) fruit hulls for methylene blue adsorption. J Taiwan Inst Chem Eng 74:96–104

Jawad AH, Abd Rashid R, Mahmuod RMA, Ishak MAM, Kasim NN, Ismail K (2015) Adsorption of methylene blue onto coconut (*Cocos nucifera*) leaf: optimization, isotherm and kinetic studies. Desalin Water Treat 57:8839–8853

Jawad AH, Ishak MAM, Farhan AM, Ismail K (2017) Response surface methodology approach for optimization of color removal and COD reduction of methylene blue using microwave-induced NaOH activated carbon from biomass waste. Desalin Water Treat 62:208–220

Jiao C, Tao J, Xiong J, Wang X, Zhang D, Lin H, Chen Y (2017) In situ synthesis of MnO_2-loaded biocomposite based on microcrystalline cellulose for Pb^{2+} removal from wastewater. Cellulose 24:2591–2604

Jinbao L, Huijuan X, Meiyun Z, Hai W, Yangyu R, Yun J (2013) Enhancement of cellulose acid hydrolysis selectivity usingmetal ion catalysts. Curr Org Chem 17:1617–1623

Jorgetto AO, Silva RIV, Longo MM, Saeki MJ, Padilha PM, Martines MAU, Rocha BP, Castro GR (2013) Incorporation of dithiooxamide as a complexing agent into cellulose for the removal and pre-concentration of Cu(II) and Cd(II) ions from natural water samples. Appl Surf Sci 264:368–374

Kanissery RG, Sims GK (2011) Biostimulation for the enhanced degradation of herbicides in soil Appl. Environ. Soil Sci. 2011, 843450. http://dx.doi.org/10.1155/2011/843450

Krutz LJ, Sensemana SA, Dozierb MC, Hoffmanc DW, Tierney DP (2003) Infiltration and adsorption of dissolved atrazine and atrazine metabolites in buffalograss filter strips JEQ 32:2319–2324

Langmuir I (1918) The adsorption of gases on plane surfaces of glass, mica and platinum. J Am Chem Soc 40:1361–1403

Liu J, Pan D, Wu X, Chen H, Cao H, Li QX, Hua R (2018) Enhanced degradation of prometryn and other s-triazine herbicides in pure cultures and wastewater by polyvinyl alcohol-sodium alginate immobilized *Leucobacter* sp. JW-1. Sci Total Environ 615:78–86

Lu Q, Tang L, Lin F, Wang S, Chen Y, Chen X, Huang B (2014) Preparation and characterization of cellulose nanocrystals via ultrasonication-assisted $FeCl_3$-catalyzed hydrolysis. Cellulose 21:3497–3506

Martins AC, Pezoti O, Cazetta AL, Bedin KC, Yamazaki DAS, Bandoch GFG, Asefa T, Visentainer JV, Almeida VC (2015) Removal of tetracycline by NaOH-activated carbon produced from macadamia nut shells: kinetic and equilibrium studies. Chem Eng J 260:291–299

Matby L, Arnold D, Arts G, Davies J, Haimbach F, Pickl C, Polusen V (2009) Aquatic macrophyte risk assessment for pesticides, 1st edn. CRC Press, Boca Raton

Miao C, Hamad WY (2013) Cellulose reinforced polymer composites and nanocomposites: a critical review. Cellulose 20:2221–2262

Mohammad A-T, Abdulhameed AS, Jawad AH (2019) Box-Behnken design to optimize the synthesis of new cross-linked chitosan-glyoxal/TiO_2 nanocomposite: methylene orange adsorption and mechanism studies. Int J Biol Macromol 129:98–109

Nawaz K, Hussain K, Choudary N, Majeed A, Ilyas U, Ghani A, Lin F, Ali K, Afghan S, Raza G, Lashari MI (2011) Eco-friendly role of biodegradation against agricultural pesticides hazards. Afr J Microbiol Res 5:177–183

Njoku VO, Islam MA, Asif M, Hameed BH (2014) Preparation of mesoporous activated carbon from coconut frond for the adsorption of Carbofuran insecticide. J Anal Appl Pyrol 110:172–180

Okumus V, Celik KS, Ozdemir S, Dundar A, Kilinc E (2015) Biosorption of chlorophenoxy acid herbicides from aqueous solution by using low-cost agricultural wastes. Desalin Water Treat 56:1898–1907

Park Y, Ayoko GA, Frost RL (2011) Application of organoclays for the adsorption of recalcitrant organic molecules from aqueous media. J Colloid Interface Sci 354:292–305

Pelosi BT, Lima LKS, Vieira MGA (2014) Removal of the synthetic dye Remazol Brilliant Blue R from textile industry wastewaters by biosorption on the macrophyte Salvinia natans. Braz J Chem Eng 31:1035–1045

Peña A, Palma R, Mingorance MD (2011) Transport of dimethoate through a Mediterranean soil under flowing surfactant solutions and treated wastewater. Coll Surf A Physicochem Eng Aspects 384:507–512

Plakas KV, Karabelas AJ (2009) Triazine retention by nanofiltration in the presence of organic matter: the role of humic substance characteristics. J Membr Sci 336:86–100

Pyrzynska K (2011) Carbon nanotubes as sorbents in the analysis of pesticides. Chemosphere 83:1407–1413

Pyrzynska K, Stafiej A, Biesaga M (2007) Sorption behavior of acidic herbicides on carbon nanotubes. Microchim Acta 159:293–298

Ren L, ZhangJ Li Y, Zhang C (2011) Preparation and evaluation of cattail fiber-based activated carbon for 2,4-dichlorophenol and 2,4,6-trichlorophenol removal. Chem Eng J 168:553–561

Salman JM, Hameed BH (2010a) Adsorption of 2,4-dichlorophenoxyacetic acid and *Carbofuran pesticides* onto granular activated carbon. Desalin 256:129–135

Salman JM, Hameed BH (2010b) Removal of insecticide carbofuran from aqueous solutions by banana stalks activated carbon. J Hazard Mater 176:814–819

Salman JM, Njoku VO, Hameed BH (2011) Bentazon and carbofuran adsorption onto date seed activated carbon: kinetics and equilibrium. Chem Eng J 173:361–368

Scribner EA, Thurman EM, Goolsby DA, Meyer MT, Battaglin, WA, Kolpin D.W.S.I.R., U.S. Geological Survey, Reston, Virginia (2005) Summary of significant results from studies of triazine herbicides and their degradation products in surface water, ground water, and precipitation in the midwestern United States during the 1990s. Scientific Investigations Report U.S. Geological Survey, Reston, Virginia

Silva LS, Lima LCB, Silva FC, Matos JME, Santos MRMC, Santos Júnior LS, Sousa KS, da Silva Filho EC (2013) Dye anionic sorption in aqueous solution onto a cellulose surface chemically modified with aminoethanethiol. Chem Eng J 218:89–98

Sun C, Huang Z, Wang J, Rao L, Zhang J, Yu J, Du J, Xu C (2016) Modification of microcrystalline cellulose with pyridone derivatives for removal of cationic dyes from aqueous solutions. Cellulose 23:2917–2927

Tan CHC, Sabar S, Hussin MH (2018) Development of immobilized microcrystalline cellulose as an effective adsorbent for methylene blue dye removal. S Afr J Chem Eng 26:11–24

Trache D, Hussin MH, Hui Chuin CT, Sabar S, Fazita MRN, Taiwo OFA (2016) Microcrystalline cellulose: isolation, characterization and bio-composites application—a review. Int J Biol Macromol 93:789–804

Velisek J, Stara A, Koutnik D, Machova J (2015) Effects of Prometryn on early life stages of common carp (*Cyprinus carpio* L.). Pestic Biochem Physiol 118:58–63

Vieira Ferreira LF, Ferreira DP, Duarte P, Oliveira A, Torres E, Ferreira Machado I, Almeida P, Reis LV, Santos PF (2012) Surface photochemistry: 3,3′-dialkylthia and selenocarbocyanine dyes adsorbed onto microcrystalline cellulose. Int J Mol Sci 13:596–611

Yonli AH, Batonneau-Gener I, Koulidiati J (2012) Adsorptive removal of α-endosulfan from water by hydrophobic zeolites. An isothermal study. J Hazard Mater 203:357–362

Zhou JH, Hu F, Jiao JG, Liu MQ, Li HX (2012) Effects of bacterial-feeding nematodes and prometryne-degrading bacteria on the dissipation of Prometryn in contaminated soil. J Soils Sedim 12:576–585